International Journal of Automotive Technology, Vol. 16, No. 5, pp. 885−893 (2015)
DOI 10.1007/s12239−015−0090−6

pISSN 1229−9138/ eISSN 1976−3832

OPTIMAL PARTITION LAYOUT OF EXPANSION CHAMBER MUFFLER WITH OFFSET INLET/OUTLET

G. W. JANG[1)] and J. W. LEE[2)*]

[1)]Faculty of Mechanical and Aerospace Engineering, Sejong University, Seoul 143-747, Korea
[2)]Division of Mechanical Engineering, Ajou University, Gyeonggi 443-749, Korea

(Received 23 October 2014; Revised 2 February 2015; Accepted 6 February 2015)

ABSTRACT−An optimal partition layout inside an expansion chamber muffler with an offset inlet/outlet is systematically designed by using topology optimization to achieve the desired characteristics in terms of acoustics and fluid mechanics. To that end, a partition volume minimization problem is formulated by applying acoustical and flow topology optimization methods. The partition volume is set as an objective function with constraints imposed on the target values of the transmission loss and pressure drop. The finite element method is employed for the acoustical and flow analyses. A design variable is assigned to each finite element such that it changes continuously between 0 and 1 to determine the state of the associated finite element. The design variables are updated during the optimization process and parameterized to converge to 0 or 1 at the end of the process. Finite elements with design variables of 1 build up rigid partitions which are optimally placed to achieve the target values of transmission loss and pressure drop. Different optimal partition layouts are obtained depending on the target frequency, the target values of transmission loss and pressure drop, and the initial values of the design variables. An experiment-based validation strongly supports the validity of the proposed muffler design method.

KEY WORDS : Muffler design, Topology optimization, Transmission loss, Pressure drop

1. INTRODUCTION

Expansion chamber mufflers with an offset inlet/outlet have been widely used to reduce flow noise in a duct such as the exhaust system of an automobile (Song and Choi, 2009; Jiang *et al.*, 2010; Munjal, 1998). Inside a muffler, partitions are inserted to improve the acoustical attenuation performance in the frequency range of interest. The noise reduction capability of a muffler is evaluated by the transmission loss (TL) in the frequency domain. To date, many efforts have been made to theoretically and numerically predict the value of the transmission loss (Munjal, 1987; Selamet and Ji, 1998a; Selamet and Ji, 1998b; Selamet *et al.*, 1998) and to maximize the transmission loss in the frequency range of interest (Lee and Jang, 2011; Ih *et al.*, 2011). However, a more recent requirement for a muffler in terms of the sound quality of an automobile is the design of an optimal partition layout to achieve a target transmission loss in the frequency range of interest, rather than to maximize the transmission loss value (Lee *et al.*, 2003; Genuit, 2004).

Conventional design methods, developed for concentric expansion chamber mufflers, are difficult to apply to an expansion chamber muffler with an offset inlet/outlet. Due to the offset of the center lines of the inlet and outlet, muffler designers are forced to consider the optimal flow path to minimize the pressure drop, in addition to the noise reduction. From the standpoint of reducing the pressure drop, partitions that attenuate the noise should not be positioned in the optimal flow path. It is also known that the pressure drop caused by the partitions in the expansion chamber is inevitable even if those partitions do not intrude into the optimal flow path (Wagh *et al.*, 2010; Lu *et al.*, 2013). Therefore, the pressure drop should be constrained in an appropriate manner to prevent the extreme pressure drop caused by the partitions when a muffler with an offset inlet/outlet is to be designed.

Design methods based on numerical simulation have made major contributions to the systematic design of mufflers. Barbieri *et al.* used shape optimization combined with the finite element method to design a reactive muffler (Barbieri *et al.*, 2004; Barbieri and Barbieri, 2006, 2012; Fonseca de Lima *et al.*, 2011). Chiu *et al.* applied a genetic algorithm or a simulated annealing method to muffler design problems (Chang and Chiu, 2008; Chiu, 2010a; Chiu, 2010b; Chiu, 2013). Although their approaches dramatically increase the transmission loss in the frequency range of interest, they require moderate initial shapes, which are difficult to select without the necessary experience or great intuition on the part of the designer. Recently, to deal with the shortcomings of shape optimization based muffler

*Corresponding author. e-mail: jinwoolee@ajou.ac.kr

design methods, Lee and Kim (2009a) introduced topology optimization to muffler design problems. Because the topology optimization approach starts from a highly simplified design domain, the result is less dependent on the designer's intuition and experience. Although Lee and Kim demonstrated the feasibility of applying topology optimization to the design of an expansion chamber muffler, their approach is capable only of maximizing the transmission loss without considering the pressure drop. Also, since their formulation was developed for a concentric expansion chamber muffler, the flow passage was set as a non-design domain and as a straight channel from the inlet to the outlet.

In this study, we present a new topology optimization formulation to design an expansion chamber muffler with an offset inlet/outlet. To take the pressure drop into account in the optimization formulation, not only an acoustical analysis but also a flow analysis is conducted to calculate the pressure drop between the inlet and the outlet. To this end, acoustical and flow analyses share the same finite element models and design variables. The material properties of each finite element for the acoustical and flow analyses are interpolated by using the same design variable. To achieve the target transmission loss and target pressure drop, both the transmission loss and the pressure drop are dealt with as inequality-type design constraints. The volume of the partitions is set as the design objective. Lee and Jang (2012) applied a multi-objective problem formulation to minimize the pressure drop and maximize the transmission loss, simultaneously. Compared to their approach, the proposed single objective formulation with constraints on the pressure drop and transmission loss is more intuitive and much easier for designers to implement, because target values for the acoustical and fluid performances can be directly specified. The formulated topology optimization problem is solved by using a gradient-based optimization scheme. The effectiveness of the proposed design method is verified by experiment, demonstrating the agreement between the measured transmission loss of a fabricated muffler and the calculated transmission loss of an optimal topology.

2. MUFFLER DESIGN PROBLEM FORMULATION

As shown in Figure 1 (a), an expansion chamber muffler considered in the present design problem consists of an inlet, an expansion chamber and an outlet. The centers of the inlet and outlet are parallel but displaced from the center of the expansion chamber in opposite directions. The z-directional depth of the muffler is assumed to be small compared with its height (d) and length (l), so that the muffler could be regarded as a 2-dimensional acoustic device. The expansion chamber is set as the design domain in which partitions are to be optimally placed, and the inlet and outlet are treated as being the non-design domain, that is, the fixed fluid region, as shown in Figure 1 (b).

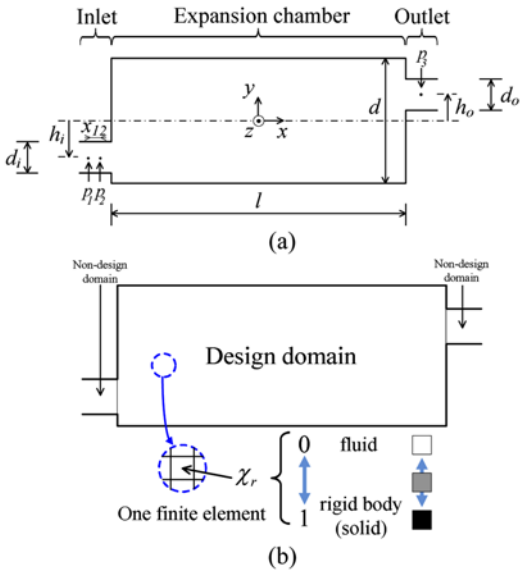

Figure 1. Expansion chamber muffler with offset inlet/outlet: (a) Analysis model; and (b) Finite element model (one design variable is assigned to each finite element in design domain).

The finite element method is employed to calculate the acoustical and flow characteristics of the muffler shown in Figure 1 (b). For the acoustical analysis, the Helmholtz equation is used for the finite element formulation. For the flow analysis, the Stokes equation is solved under the assumption that the input flow is very slow. To that end, the finite element approximation procedure described in the previous work (Lee and Jang, 2012) is recalled.

2.1. Finite Element Equation for Acoustical Analysis

The acoustic pressure p^H inside an acoustic device such as the muffler shown in Figure 1 (a) is governed by the Helmholtz equation (Lee and Kim, 2009b):

$$\nabla\cdot\left(\frac{1}{\rho}\nabla p^H\right)+\frac{\omega^2}{K}p^H=0,\quad \omega=2\pi f, \tag{1}$$

where ρ denotes the density; ω, the angular frequency; f, the frequency; and K, the bulk modulus ($K=\rho c^2$, c: speed of sound in the acoustic medium). The particle velocity $\vec{u}$ and the acoustic pressure are related by the linearized Euler's equation:

$$\vec{u}=-\frac{1}{j\rho\omega}\nabla p^H, \tag{2}$$

where $j=\sqrt{-1}$.

To calculate the TL value at the target frequency, the following boundary conditions are imposed on each boundary:

$u_x=1$ for the inlet, (3a)

$$p^H/u_x = \rho c \quad \text{for the outlet,} \tag{3b}$$

$$\frac{\partial p^H}{\partial m} = 0 \quad \text{for the other boundaries,} \tag{3c}$$

where u_x is the x component of the particle velocity. Under the assumption that only plane acoustic waves are progressing in the inlet and outlet, the particle velocity of the unit magnitude in Equation (3a) is imposed on the inlet, and the anechoic termination condition in Equation (3b) is imposed on the outlet. The rigid wall boundary condition in Equation (3c) is imposed on the other boundaries where the normal direction of the boundary is denoted by m.

The matrix form of the finite element equation for the Helmholtz equation described in Equation (1) with the boundary conditions described in Equation (3) can be written as

$$[\mathbf{K}^H - \omega^2 \mathbf{M}^H]\mathbf{P}^H = \mathbf{F}^H, \tag{4}$$

where $\mathbf{P}^H$ and $\mathbf{F}^H$ are the nodal vectors of the acoustic pressure and applied equivalent force, respectively. The element stiffness matrix $\mathbf{k}_n^H$ and the element mass matrix $\mathbf{m}_n^H$ in Equation (5) are assembled to build the global stiffness and mass matrices ($\mathbf{K}^H$ and $\mathbf{M}^H$), respectively:

$$\mathbf{K}^H = \mathop{A}_{n=1}^{N} \mathbf{k}_n^H \text{ with } \mathbf{k}_n^H = \int_{\Omega_n} \frac{1}{\rho_n} (\nabla \mathbf{N}_n^H)^{\mathrm{T}} \nabla \mathbf{N}_n^H d\Omega, \tag{5a}$$

$$\mathbf{M}^H = \mathop{A}_{n=1}^{N} \mathbf{m}_n^H \text{ with } \mathbf{m}_n^H = \int_{\Omega_n} \frac{1}{K_n} (\mathbf{N}_n^H)^{\mathrm{T}} \mathbf{N}_n^H d\Omega, \tag{5b}$$

where $\mathbf{N}_n^H$ is the shape function matrix of the n-th finite element, $\mathop{\mathbf{A}}_{n=1}^{N}$ represents the finite element assembly operator, and N is the total number of elements. The equivalent force vector $\mathbf{F}^H$ is represented by assembling the element force matrices $\mathbf{f}^H$ specified in the inlet boundary:

$$\mathbf{F}^H = \mathop{A}_{n=1}^{N} \mathbf{f}_n^H \text{ with } \mathbf{f}^H = -j\omega \int_{\partial\Omega_n^{in}} \mathbf{N}_n^H d(\partial\Omega), \tag{6}$$

where $\partial\Omega_n^{\text{in}}$ is the inlet boundary of element n, and N^{in} is the number of associated elements. The anechoic termination condition given by Equation (3b) affects the mass matrices of the elements lying on the outlet:

$$\mathbf{m}_n^H = \int_{\Omega_n} \frac{1}{K_n} (\mathbf{N}_n^H)^T \mathbf{N}_n^T d\Omega + \frac{1}{j\omega} \int_{\partial\Omega_n^{\text{out}}} \frac{1}{\rho_n c_n} (\mathbf{N}_n^H)^T \mathbf{N}_n^H d(\partial\Omega), \tag{7}$$

where Ω_n is the element area and $\partial\Omega_n^{\text{out}}$ is the outlet boundary of element n.

The transmission loss of a muffler is calculated by using the three-point method (Wu and Wan, 1996):

$$TL(f) = 20 \cdot \log_{10} \left| \frac{1}{p_3^H} \frac{p_1^H - p_2^H \cdot e^{-jk \cdot x_{12}}}{1 - e^{-jk \cdot 2x_{12}}} \right|, \; k = \frac{2\pi f}{c}, \tag{8}$$

where x_{12} is the distance between two points in the inlet, and p_1^H, p_2^H, and p_3^H are the acoustic pressures at two points in the inlet and at one point in the outlet (see Figure 1 (a)).

2.2. Finite Element Equation for Flow Analysis

The Stokes equation, modified for topology optimization of an incompressible Newtonian fluid with a constant viscosity, is given as (Borrvall and Peterson, 2003)

$$-\nabla \cdot (\mu \nabla \mathbf{v}^s) + \nabla p^s + \gamma \mathbf{v}^s = \mathbf{0}, \tag{9a}$$

$$\nabla \cdot \mathbf{v}^s = 0, \tag{9b}$$

where p^s is the pressure, $\mathbf{v}^S = \{v_x^S, v_y^S\}^T$ is the fluid velocity vector, and μ is the viscosity. No body force is considered in the above equations for the present muffler analysis. In Equation (9a), the inverse permeability γ is introduced to represent the state of an element depending on the value of the associated design variable. The parameterization for γ will be presented in the topology optimization formulation section, below. A quadratic velocity profile (a Hagen-Poiseuille flow) with a unit central magnitude is given on the inlet, and a zero pressure is imposed on the outlet. No slip boundary condition is used on the other boundaries.

The finite element equation for the Stokes equation given in Equation (9) is expressed as a mixed formulation for velocity and pressure:

$$\mathbf{K}^S \mathbf{U}^S = \mathbf{F}^S, \tag{10}$$

$$\mathbf{U}^S = \{\mathbf{V}^S \; \mathbf{P}^S\}^{\mathrm{T}}, \text{ and } \mathbf{F}^S = \mathbf{0}, \tag{11}$$

where $\mathbf{U}^S$ consists of the nodal vectors of velocity and pressure ($\mathbf{V}^S$ and $\mathbf{P}^S$). The global stiffness matrix $\mathbf{K}^S$ is obtained by assembling the element stiffness matrix $\mathbf{k}_n^S$ in Equation (12a):

$$K^S = \mathop{A}_{n=1}^{N} \mathbf{k}_n^S \text{ with } \mathbf{k}_n^S = \begin{bmatrix} \mathbf{k}_{vv} & \mathbf{k}_{vp} \\ \mathbf{k}_{vp}^T & \mathbf{0} \end{bmatrix}, \tag{12a}$$

$$\mathbf{k}_{vv} = \int_{\Omega_n} [\mu \mathbf{C}^T \mathbf{C} + \gamma (\mathbf{N}_v^s)^T \mathbf{N}_v^s] d\Omega \text{ with } \mathbf{C} = \begin{bmatrix} \partial/\partial x & \partial/\partial y & 0 & 0 \\ 0 & 0 & \partial/\partial x & \partial/\partial y \end{bmatrix}^T \mathbf{N}_v^S, \tag{12b}$$

$$\mathbf{k}_{vp} = \int_{\Omega_n} \mathbf{E}^T \mathbf{N}_p^s d\Omega \text{ with } \mathbf{E} = [\partial/\partial x \quad \partial/\partial y] \mathbf{N}_v^S, \tag{12c}$$

where $\mathbf{N}_v^S$ and $\mathbf{N}_p^S$ are shape function matrices. It is recommended that the order of the shape functions for the velocity be higher than that for the pressure (for this study, bilinear functions are used for the velocity, and constant shapes are used for the pressure.).

The pressure drop across the muffler shown in Figure 1 (b) is obtained as the difference between the pressure values at the inlet and the outlet:

$$\Delta p^s = p_{\text{inlet}}^s - p_{\text{outlet}}^s, \tag{13}$$

where p_{outlet}^s is set to zero in this investigation, and p_{inlet}^s should be calculated by using Equations (10) to (13).

2.3. Topology Optimization Method

In this study, the acoustical and flow topology optimization methods are used separately with the same design variable

assigned to one finite element. The state of each finite element is determined by applying appropriately selected interpolation functions (or parameterizations) and the value of the associated design variable which is updated during the optimization. The interpolation functions should be selected by considering the design goal and the physics used in the formulated optimization problem. Since the present formulation involves the simultaneous use of two topology optimization methods, two groups of interpolation functions are used. The first group determines the density and bulk modulus of each finite element in the acoustical topology optimization. The second group of interpolation function determines the permeability of each finite element in the flow topology optimization.

As shown in Figure 1 (b), the design variable χ_r is assigned to each finite element in the design domain and changes continuously between 0 and 1. The same finite element model is used for acoustical and flow topology optimization. The state of the associated finite element changes with the assigned design variable: it is filled with air (fluid) for $\chi_r = 0$, it is regarded as a rigid body (solid) for $\chi_r = 1$, and it is filled with an intermediate material for $0 < \chi_r < 1$:

$$1/\rho(\chi_r) = 1/\rho_{\text{air}} + \chi_r(1/\rho_{\text{rigid}} - 1/\rho_{\text{air}}), \tag{14a}$$

$$1/K(\chi_r) = 1/K_{\text{air}} + \chi_r(1/K_{\text{rigid}} - 1/K_{\text{air}}), \tag{14b}$$

$$\gamma_r(\chi_r) = \gamma_{\text{fluid}} + (\gamma_{\text{solid}} - \gamma_{\text{fluid}}) \cdot \chi_r \frac{1+q}{\chi_r + q}, \tag{15}$$

where the subscripts “air” and “rigid” in Equations (14a) and (14b) indicate the air and rigid body materials, respectively, in the acoustical topology optimization. In Equation (15), “fluid” and “solid” denote the solid and fluid materials in the flow topology optimization. The interpolation functions in Equations (14) and (15) have been validated for acoustical and flow topology optimization problems in previous investigations (Lee and Kim, 2009a; Lee, 2015; Lee and Jang, 2012). To facilitate the convergence of the design variable to 0 or 1, the interpolation for flow topology optimization in Equation (15) requires the use of penalty parameter q. In this study, the proper value of q is determined by pre-study: $q = 0.1$.

The acoustic wave transmission of a finite element in acoustical topology optimization and the fluid passage of the element in flow topology optimization are determined by the assigned design variable χ_r. Because the associated element is filled with air (fluid) for $\chi_r = 0$, an incident acoustic wave to the finite element is transmitted to the other side and incoming fluid passes through the finite element. For $\chi_r = 1$, the associated element is filled with a rigid body (solid) whose density, bulk modulus and inverse permeability are extremely high compared with those of air (fluid). The rigid body elements totally reflect any incident acoustic wave, and the flow velocity on the element is almost zero if γ_{solid} is set to a very large value. Accordingly, the rigid body elements (solid elements) build up partitions inside an expansion chamber in the topology optimization.

To allow the constrained values of transmission loss at the target frequencies and pressure drop by using only small amount of partition volume, the volume of the partitions is selected as the design objective while the values of transmission loss and pressure drop are set as design constraints:

$$\min_{0 \le \chi_r \le 1} L_{\text{obj}} = \sum_{r=1}^{R} \chi_r \tag{16}$$

$$TL_{f=f_t} \ge TL_{target}, \ (t = 1, 2, \ldots, T) \tag{17a}$$

$$\Delta p^s \le \Delta p^s_{\text{target}}, \tag{17b}$$

where R is the total number of design variables. In Equation (17a), $TL_{f=f_t}$ denotes the transmission loss at the target frequency (f_t), TL_{target} is the target transmission loss value, and T is the total number of target frequencies. In Equation (17b), $\Delta p^s_{\text{target}}$ represents the target pressure drop value. Since finite elements with $\chi_r = 1$ build up rigid partitions, the design objective in Equation (16) represents the partition volume. Note that the optimization formulation is set differently in the previous researches (Lee and Kim, 2009a; Lee and Jang, 2012). That is, the partition-volume-minimization problem formulated for this investigation of muffler design consists of one objective function in Equation (16), two inequality constraint conditions in Equation (17), and three equality constraint conditions in Equations (14) to (15).

3. NUMERICAL RESULTS AND EXPERIMENTAL VALIDATION

Figure 2 illustrates the process for solving the formulated muffler design problem. The specific values of the symbols used to solve the present optimization problem are listed in Table 1. The fluid in this work is assumed to be air. The values for the density and the speed of sound in a rigid body element are determined by the criteria suggested by Lee and Kim (Lee and Kim, 2009c), and the value used in the previous work (Borrvall and Peterson, 2003) is used as the inverse permeability of the solid. The design domain shown in Figure 1 is discretized by using 1500 four-node rectangular elements with the size of $0.01\ m \times 0.005\ m$. The design variables are updated by using the method of moving asymptotes (Svanberg, 1987) for which the entire analysis and optimization are implemented by using Matlab. The method of moving asymptotes requires the sensitivity analysis on the constraints as well as the objective function with respect to each design variable as shown in the flow chart of Figure 2.

It is expected that the optimal topologies would be affected by TL_{target} and f_t in Equation (17a), $\Delta p^s_{\text{target}}$ in Equation (17b), and by the initial values of design variable (χ_r^{ini}) in Equations (14) and (15). To investigate these effects, the optimal topologies for various values of TL_{target} are obtained (Case A). Then the effects of f_t, $\Delta p^s_{\text{target}}$ and χ_r^{ini}

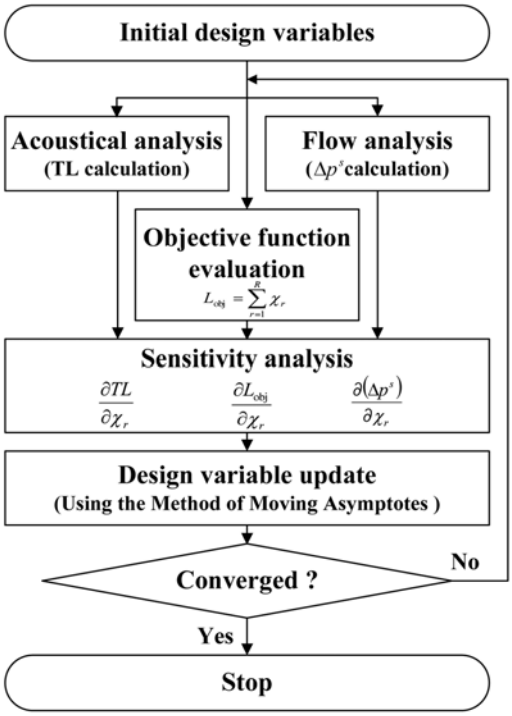

Figure 2. Flow chart for solving the formulated muffler design problem shown in Equations (14) to (17).

Table 1. Specific values used in muffler design problem.

Symbol	Quantity	Value
l	Length of expansion chamber	0.5 m
d	Height of expansion chamber	0.15 m
d_i	Height of inlet	0.04 m
d_o	Height of outlet	0.04 m
h_i	Distance between centers of the expansion chamber and inlet	0.035 m
h_o	Distance between centers of the expansion chamber and outlet	0.025 m
x_{12}	Distance between two measurement points in inlet	0.01 m
ρ_{air}	Density of air	1.21 kg/m^3
c_{air}	Speed of sound in air	343 m/s
ρ_{rigld}	Density of rigid body	$10^7 \cdot \rho_{rigid}$
c_{rigld}	Speed of sound in rigid body	$10^1 \cdot c_{rigid}$

on the optimal topologies are investigated (Case B). The total number of design variables is 1,500 in all case studies: R = 1,500.

For the optimizations described in Case A, the formulated problem is solved by using different values for the target transmission loss (TL_{target} = 10,15,20,25 dB) while keeping the other parameters fixed; three target frequencies are used, namely, f_1 = 650 Hz, f_2 = 700 Hz, and f_3 = 750 Hz, and the target pressure drop and initial design values are given as $\Delta p^s_{\text{target}}$ = 7.0 Pa and χ_r^{ini} = 0.5, respectively. Figure 3 shows the optimized partition layouts for different target transmission loss values. In each optimal topology, the black areas represent the partitions occupied by rigid body (solid) elements. Note that more rigid body elements are used in the final topologies as the value of TL_{target} increases: L_{obj} = 28 for TL_{target} = 10 dB in Case A-1, L_{obj} = 29 for TL_{target} = 15 dB in Case A-2, L_{obj} = 46 for TL_{target} = 10 dB in Case A-3, and L_{obj} = 52 for TL_{target} = 25 bB in Case A-4. In addition, the partition layouts differ depending on the value of TL_{target}. While Figures 3 (a), 3 (c), and 3(d) show two partitions being built up from the top and bottom walls, only one partition appears in Figure 3 (b). Figure 4 compares the transmission loss curves of the optimal topologies with that of the reference muffler, which does not have a partition in the expansion chamber. Note that, in Figure 4, the low transmission loss of the reference muffler at the target frequency is increased considerably in the optimized mufflers as a result of the optimally-placed partitions. Figure 5 shows the optimization history for the result obtained for Case A-4. Figure 5 (a) shows the convergence of the design objective, while Figure 5 (b) shows the change in the transmission loss at the target

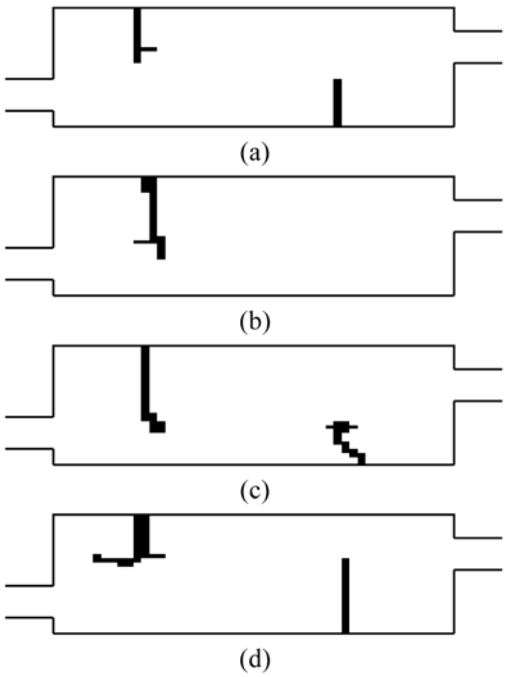

Figure 3. Optimized partition layouts for different target transmission loss values (target frequencies, f_1 = 650 Hz, f_2 = 700 Hz and f_3 = 750 Hz, $\Delta p^s_{\text{target}}$ = 7.0 Pa and χ_r^{ini} = 0.5 are set fixed.): (a) TL_{target} = 10 dB (Case A-1); (b) TL_{target} = 15 dB (Case A-2); (c) TL_{target} = 20 dB (Case A-3); and (d) TL_{target} = 25 dB (Case A-4).

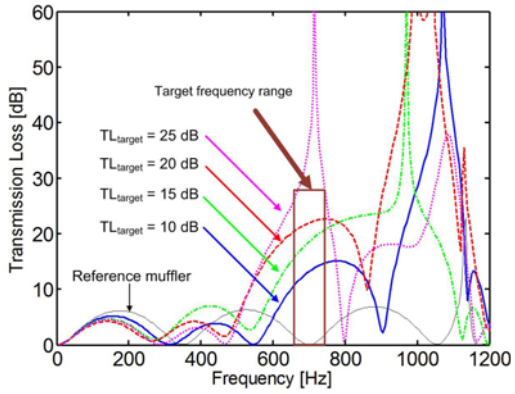

Figure 4. Transmission loss curves for optimized partition layouts shown in Figure 3 and reference muffler, with no partitions in expansion chamber.

frequencies, as well as the pressure drop during optimization.

For the optimizations of Case B, to investigate the effect of f_i, $\Delta p^s_{\text{target}}$, and χ_r^{ini}, the formulated problem is solved repeatedly by using a set of (f_i, $\Delta p^s_{\text{target}}$, χ_r^{ini}) that is different from that used for Case A. In Case B-1, the target frequencies are set to f_1 = 450 Hz, f_2 = 500 Hz, and f_3 = 550 Hz while the other parameters are the same as in Case A-1

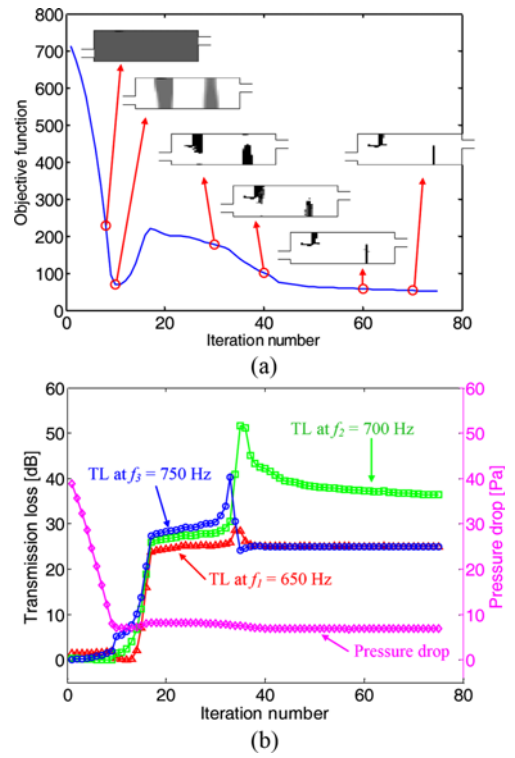

Figure 5. Optimization history for result shown in Figure 3 (d): (a) History of objective function value with several intermediate state topologies; and (b) Comparison of TL values at target frequencies and pressure drop during optimization process.

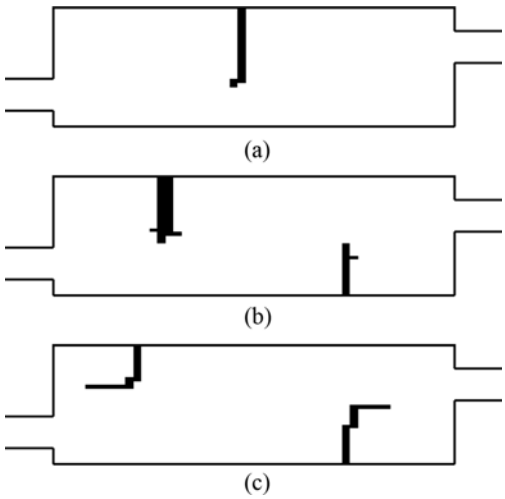

Figure 6. Optimal topologies obtained to investigate the effect of target frequencies, initial value of design variable, and target pressure drop on optimal partition layout. (a) Case B-1; (b) Case B-2 and (c) Case B-3.

(TL_{target} = 10 dB, χ_r^{ini} = 0.5 and $\Delta p^s_{\text{target}}$ = 7.0 Pa). In Case B-2, a set of χ_r^{ini} = 0.0 is used as initial design variables while the other parameters are the same as in Case A-2 ($\Delta p^s_{\text{target}}$ = 15 dB, f_1 = 650 Hz, f_2 = 700 Hz, f_3 = 750 Hz, and $\Delta p^s_{\text{target}}$ = 7.0 Pa). In Case B-3, only the pressure drop changes, from 7.0 Pa to 6.5 Pa, while the other parameters are kept the same as in Case A-4 (TL_{target} = 25 dB, f_1 = 650 Hz, f_2 = 700 Hz, f_3 = 750 Hz, and χ_r^{ini} = 0.5).

The optimal topologies obtained in Cases B-1, B-2, and B-3 are shown in Figure 6. The effect of the target frequency on the optimal topology can be shown by comparing Figure 3 (a) and Figure 6 (a); while only one partition is built up around the center of the upper wall in Figure 6 (a) (f_1 = 450 Hz, f_2 = 500 Hz, f_3 = 550 Hz), two partitions from both the upper and lower walls are obtained as shown in Figure 3 (a) (f_1 = 650 Hz, f_2 = 700 Hz, f_3 = 750 Hz). A comparison of Figure 3 (b) and Figure 6 (b) shows that the use of different initial design values can lead to different optimal topologies. Because the present optimization was solved by using MMA (Svanberg, 1987), a gradient-based optimizer, the obtained results may be mostly local optima. Thus, the dependency of the optimum results on initial design variables is inevitable. Note that, despite there being a major topology difference between the results shown in Figure 3 (b) and Figure 6 (b), they produce have the similar transmission loss and pressure drop values at the same target frequencies. By reducing the target pressure drop value, the optimal partition layout shown in Figure 3 (d) changes to the result shown in Figure 6 (c) where it can be seen that the end of the right partition is bent to satisfy the stricter constraint on the pressure drop.

These results imply that the proposed muffler design method can provide muffler designers with many options for the design of an expansion chamber muffler with an

offset inlet/outlet. A range of optimal partition layouts can be obtained by choosing a different set of the four parameters, that is, TL_{target}, f_t, $\Delta p^s_{\text{target}}$, and χ_r^{ini}, which are called as design parameters hereafter. Sometimes, the optimal topology obtained for selected parameter values may not have a satisfactorily reduced design objective. In such a case, an improved solution could be obtained by slightly changing one or two of the design parameters. For example, when a small pressure drop has higher design priority than a high transmission loss, the designers could obtain a better partition layout by adjusting only the target values for the pressure drop and transmission loss in the frequency range of interest.

To validate the proposed design method, the acrylic muffler shown in Figure 7 (a) was fabricated based on the optimal topology given in Figure 6 (a). The depth of the muffler was set to 40 mm, and the optimal topology for the partitions, shown in Figure 6 (a), was extruded along the z-axis of the acrylic muffler. Figure 7 (b) shows four microphones (46BE, G. R. A. S., Denmark) installed to measure the transmission loss, and one horn driver (DU-75, Inter-M, Korea) which was used to provide the incident acoustic pressure into the inlet. The sound transmission loss module of LMS Test Lab (Siemens, Germany) was used for the sound generation and data acquisition with signal processing. The horn driver was actuated by a burst random signal and the measured transmission loss was averaged over 25 times with a frequency resolution of 1.5625 Hz. Figure 8 shows that the measured transmission loss for the acrylic muffler shown in Figure 7 (a) is in good agreement with numerical result obtained for the optimal topology shown in Figure 6 (a). Thus, the proposed muffler design method is very effective for increasing the transmission loss in the frequency range of interest in an actual muffler system in which the center lines of the inlet and outlet are parallel but displaced from the center of the expansion chamber.

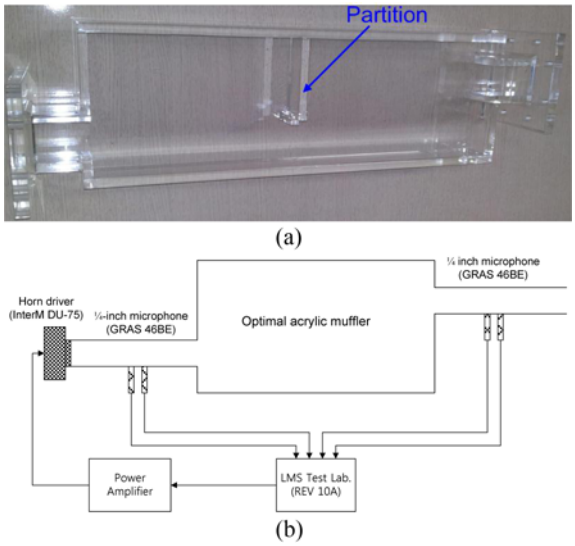

Figure 7. Experimental validation: (a) Fabricated acrylic muffler based on optimal topology shown in Figure 6 (a), and (b) Experimental set-up to measure transmission loss value of acrylic muffler shown in Figure 7 (a).

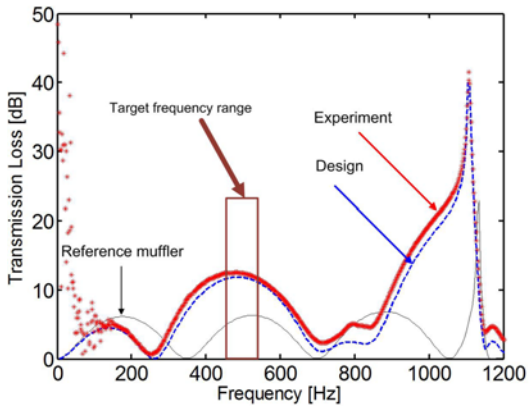

Figure 8. Comparison between measured transmission loss curve of fabricated muffler shown in Figure 7 (a) and numerically calculated transmission loss curve of the optimization result shown in Figure 6 (a).

4. CONCLUSION

A topology optimization based design problem for an expansion chamber muffler with an offset inlet/outlet was formulated by using acoustical and flow topology optimization methods. To achieve the desired acoustical and fluid characteristics for the muffler, the transmission loss values at the target frequencies and the pressure drop value between the inlet and the outlet were constrained. The partition volume was set as the design objective. The formulated design problem was solved for different sets of the design parameters: target frequencies, target transmission loss, target pressure drop, and initial design variables. The effect of each design parameter on the optimal partition layout was also investigated by comparing the resulting partition topologies before and after changing each parameter. The proposed design method was verified by experiment. The measured transmission loss of the fabricated muffler was found to be in good agreement with the calculated transmission loss for the optimal topology. Currently, our research group is carrying out the optimal design considering thermal characteristics as well as acoustical characteristics. The research results will be introduced in the near future.

The optimal partition layouts obtained in this work could give automotive engineers some intuition for optimal muffler design. As shown in case study results, partitions are placed around the nodal lines of acoustic natural modes near the target frequency and the ends of partitions starting from the walls bend not to intrude the optimal flow path. The optimal partition configuration problem for the same

amount of partition volume could have multiple solutions because it is a kind of an inverse engineering problem. The consideration of an additional design goal in the optimization formulation such as the moderate value of pressure drop could be one criteria to select the best solution among them. Furthermore, manufacturability of the optimized mufflers and consideration of more realistic boundary conditions should be dealt with for practical applicaiotns.

ACKNOWLEDGEMENT–This research was supported by the Basic Science Research Program through the National Research Foundation of Korea (NRF), funded by the Ministry of Education (No. 2013R1A1A2010158).

REFERENCES

Barbieri, R., Barbieri, N. and Fonseca de Lima, K. (2004). Application of the Galerkin-FEM and the improved four-pole parameter method to predict acoustic performance of expansion chambers. *J. Sound Vib.* **276**, **3–5**, 1101–1107.

Barbieri, R. and Barbieri, N. (2006). Finite element acoustic simulation based shape optimization of a muffler. *Appl. Acoust.* **67**, **4**, 346–357.

Barbieri, R. and Barbieri, N. (2012). The technique of active/inactive finite elements for the analysis and optimization of acoustical chambers. *Appl. Acoust.* **73**, **2**, 184–189.

Borrvall, T. and Peterson, J. (2003). Topology optimization of fluids in Stokes flow. *Int. J. Numer. Meth. Fluids*. **41**, **1**, 77–107.

Chang, Y. C. and Chiu, M. C. (2008). Shape optimization of one-chamber perforated plug/non-plug mufflers by simulated annealing method. *Int. J. Numer. Methods Eng.* **74**, **10**, 1592–1620.

Chiu, M. C. (2010). Shape optimization of multi-chamber mufflers with plug-inlet tube on a venting process by generic algorithms. *Appl. Acoust.* **71**, **6**, 495–505.

Chiu, M. C. (2010). Optimal design of multichamber mufflers hybridized with perforated intruding inlets and resonating tubes using simulated annealing. *Trans. ASME: J. Vib. Acous.* **132**, **5**, 054503-1-9.

Chiu, M. C. (2013). Numerical assessment for a broadband and tuned noise using hybrid mufflers and a simulated annealing method. *J. Sound Vib.* **332**, **12**, 2923–2940.

Fonseca de Lima, K., Lenzi, A. and Barbieri, R. (2011). The study of reactive silencers by shape and parametric optimization techniques. *Appl. Acoust.* **72**, **4**, 142–150.

Genuit, K. (2004). The sound quality of vehicle interior noise: a challenge for the NVH-engineers. *Int. J. Vehicle Noise and Vibration* **1**, **1/2**, 158–168.

Ih, J. G., Choi, C. Y., Kim, T. K., Jang, S. H. and Kim, H. J. (2011). Optimal design of the exhaust system layout to suppress the discharge noise from an idling engine. *Int. J. Automotive Technology* **12**, **4**, 617–630.

Jiang, C., Wu, T. W., Xu, M. B. and Cheng, C. Y. R. (2010). BEM modeling of mufflers with diesel particulate filters and catalytic converters. *Noise Control Eng. J.* **58**, **3**, 243–250.

Lee, J. W. (2015). Optimal topology of reactive muffler achieving target transmission loss values: Design and experiment. *Appl. Acoust.* **88**, **2**, 104–113.

Lee, J. W. and Kim, Y. Y. (2009). Topology optimization of muffler internal partitions for improving acoustical attenuation performance. *Int. J. Numer. Methods Eng.* **80**, **4**, 455–477.

Lee, J. W. and Kim, Y. Y. (2009). Optimal distribution of holes in a partition interfacing two cavities for controlling the eigenfrequencies by acoustical topology optimization. *Comput. Methods Appl. Mech. Eng.* **198**, **27–29**, 2175–2189.

Lee, J. W. and Kim, Y. Y. (2009). Rigid body modeling issue in acoustical topology optimization. *Comput. Methods Appl. Mech. Eng.* **198**, **9–12**, 1017–1030.

Lee, J. W. and Jang, G. W. (2011). Systematic design of an expansion chamber muffler with offset inlet/outlet by topology optimization. *Inter-noise and Noise-con Conf. Proc.*, NoiseCon11, Portland Or, 637–641.

Lee, J. W. and Jang, G. W. (2012). Topology design of reactive mufflers for enhancing their acoustic attenuation performance and flow characteristics simultaneously. *Int. J. Numer. Methods Eng*. **91**, **5**, 552–570.

Lee, M., McCarthy, M., Romzek, M., Frei, T. and Bemman, Y. (2003). Exhaust system design for sound quality. *SAE Paper No.* 2003-01-1645.

Lu, H., Wu, T., Bai, S., Xu, K., Huang, Y., Gao, W., Yin, X. and Chen, L. (2013). Experiment on thermal uniformity and pressure drop of exhaust heat exchanger for automotive thermoelectric generator. *Energy*, **54**, 372–377.

Munjal, M. L. (1987). A simple numerical method for three-dimensional analysis of simple expansion chamber mufflers of rectangular as well as circular cross-section with a stationary medium. *J. Sound. Vib.* **116**, **1**, 71–88.

Munjal, M. L. (1998). Analysis and design of mufflers-an overview of research at the Indian Institute of Science. *J. Sound. Vib.* **211**, **3**, 425–433.

Selamet, A. and Ji, Z. L. (1998). Acoustic attenuation performance of circular expansion chambers with offset inlet/outlet: I. Analytical Approach. *J. Sound. Vib.* **213**, **4**, 601–617.

Selamet, A. and Ji, Z. L. (1998). Diametral plane-wave analysis for short circular chambers with end offset inlet/outlet and side extended inlet/outlet. *J. Sound. Vib.* **214**, **3**, 580–587.

Selamet, A., Ji, Z. L. and Radavich, P. M. (1998). Acoustic attenuation performance of circular expansion chambers with offset inlet/outlet: II. Comparison with experimental and computational studies. *J. Sound. Vib.* **213**, **4**, 619–641.

Song, B. H. and Choi, Y. H. (2009). Development of quantitative measuring technique to find critical flow conditions for preventing soot deposit accumulated in

the diesel exhaust system using main muffler composed of three chambers. *Int. J. Automotive Technology* **10**, **4**, 405–411.

Svanberg, K. (1987). The method of moving asymptotes: A new tool for structural optimization. *Int. J. Numer. Methods Eng.* **24**, **2**, 359–373.

Wagh, S., Sen, S., Iyer, G. and Shukla, S. (2010). Development of exhaust silencer for improved sound quality and optimum back pressure. *SAE Paper No.* 2010-01-0388.

Wu, T. W. and Wan, G. C. (1996). Muffler performance studies using a direct mixed-body boundary element method and a three-point method for evaluating transmission loss. *Trans. ASME: J. Vib. Acous*. **118**, **3**, 479–484.